

1 **Climate-driven change in the North Atlantic and Arctic Ocean can greatly**
2 **reduce the circulation of the North Sea**

3 **Jason Holt¹, Jeff Polton¹, John Huthnance¹, Sarah Wakelin¹, Enda O’Dea², James**
4 **Harle³, Andrew Yool³, Yuri Artioli⁴, Jerry Blackford⁴, John Siddorn², Mark Inall^{5,6}**

5 ¹National Oceanography Centre, 6 Brownlow Street, Liverpool, UK

6 ²Met Office, FitzRoy Road, Exeter, UK

7 ³National Oceanography Centre, Empress Dock, Southampton, UK

8 ⁴Plymouth Marine Laboratory, Plymouth, UK

9 ⁵Scottish Association for Marine Science, Scottish Marine Institute, Oban, UK

10 ⁶University of Edinburgh, School of Geosciences, Edinburgh,

11 Corresponding author: Jason Holt (jholt@noc.ac.uk)

12 **Key Points:**

- 13 • Potential end-of-century scenarios of dramatically reduced North Sea inflow and
14 circulation are demonstrated by downscaling experiments.
- 15 • This reduction is traced to increased shelf-slope salinity stratification and modified North
16 Atlantic and Arctic circulation and salinity.
- 17 • The North Sea then becomes more estuarine, with some regions of substantially enhanced
18 nutrient content and primary production.
19

20 Abstract

21 We demonstrate for the first time a direct oceanic link between climate-driven change in
22 the North Atlantic and Arctic oceans and the circulation of the northwest European shelf-seas.
23 Downscaled scenarios show a shutdown of the exchange between the Atlantic and the North Sea,
24 and a substantial decrease in the circulation of the North Sea in the second half of the 21st
25 Century. The northern North Sea inflow decreases from 1.2-1.3Sv ($1\text{Sv}=10^6\text{ m}^3\text{s}^{-1}$) to 0.0-0.6Sv
26 with Atlantic water largely bypassing the North Sea. This is traced to changes in oceanic haline
27 stratification and gyre structure, and to a newly identified circulation-salinity feedback. The
28 scenario presented here is of a novel potential future state for the North Sea, with wide-ranging
29 environmental management and societal impacts. Specifically, the sea would become more
30 estuarine and susceptible to anthropogenic influence with an enhanced risk of coastal
31 eutrophication.

32 Plain Language Summary

33 Little is known about how climate change might impact the long-term circulation of shelf-seas.
34 In this paper, we use a high-resolution shelf-sea model to demonstrate how end-of-century
35 changes in the wider ocean can lead to a substantial reduction in the flow of water from the
36 North Atlantic into the North Sea. This, in turn, reduces the circulation of this sea, which
37 becomes more influenced by rivers and less by oceanic waters. River water generally contains
38 higher levels of nutrients and our simulations show that this future scenario leads to enhanced
39 levels of phytoplankton growth in local regions of the North Sea. This may lead to undesirable
40 disturbances to the marine ecosystems, such as depletion of oxygen near the seabed. The reduced
41 circulation would also disrupt the transport of larvae around the sea and lead to increased
42 retention of pollutants. The reduction in circulation arises from several causes relating to
43 increased density layering at the continental shelf-edge; changes in the large-scale ocean
44 circulation and salinity; and disruption of the density-driven circulation of the North Sea. By
45 exploring these novel future scenarios, we emphasize the need to understand better the many
46 ways climate change can influence the marine environment and its ecosystems.

47 1. Introduction

48 The material properties of coastal and shelf-seas (e.g. salinity, nutrients, carbon and
49 pollutants) are largely controlled by atmospheric, oceanic and terrestrial forcing and by their
50 circulation [Gröger *et al.*, 2013; Holt *et al.*, 2012]. However, little is known about how the
51 circulation of shelf-seas might change under future climatic conditions. There have been many
52 national and international programmes exploring climate impacts in the North Sea [Quante and
53 Colijn, 2016], arising from the societal requirement to ensure and maintain its Good
54 Environmental Status and its delivery of environmental services, such as fisheries and carbon
55 sequestration [Thomas *et al.*, 2004]. To date these have largely neglected a detailed treatment of
56 the circulation and in particular the far-field oceanic impacts on this. They have focused on the
57 local density and wind driven circulation, and have shown only modest projected changes in
58 circulation generally attributed to changes in wind forcing [Schrum *et al.*, 2016]. In this paper,
59 we present downscaling shelf-sea model experiments that demonstrate the potential for a
60 substantial reduction in the North Sea circulation arising from changes in the North Atlantic and
61 Arctic Ocean. Similar changes in North Sea circulation were noted by Tinker *et al* [2016] in
62 three of their eleven downscaled ensemble members with the highest climate sensitivity, but

63 without further analysis. Here we use an analysis of regional model experiments and their
64 driving global ocean models, along with geostrophic dynamics, to explain the nature of this
65 potential shutdown in North Sea circulation (section 3.1). Linear models using ocean data from
66 the Coupled Model Intercomparison Programme phase 5 (CMIP5) ensemble [Taylor *et al.*, 2012]
67 are used to estimate the likelihood of the shutdown occurring (section 3.2). An ecosystem model
68 is used to illustrate some potential environmental implications of such a change in the North Sea
69 (section 3.3).

70 **2. Methods**

71 **2.1 Model experiment design**

72 Global coupled ocean-atmosphere climate models, as in CMIP, provide our best
73 understanding of potential future states of the ocean. However, they currently lack the resolution
74 and process representation to provide robust projections in shelf-seas [Holt *et al.*, 2017]. They
75 generally do not include tides, resolve the barotropic Rossby radius on-shelf, resolve seasonal
76 stratification or have appropriate vertical mixing schemes. These features require a downscaling
77 approach, achieved here by running a shelf-sea model forced by boundary conditions from global
78 climate models.

79 We use the AMM7 operational hydrodynamic model of the northwest European
80 continental shelf [O'Dea *et al.*, 2012], based on the NEMO V3.2 code [Madec, 2008] at ~7 km
81 resolution with 32 terrain-following vertical coordinates. Unlike other such simulations
82 [Adlandsvik, 2008; Tinker *et al.*, 2016], the domain boundaries are placed sufficiently far into the
83 ocean interior to allow ocean-shelf coupling processes to be accurately represented (Fig. 1). For
84 atmospheric forcing we use parameters from HADGEM2 [Jones *et al.*, 2011] using the CORE
85 parameterization [Large and Yeager, 2004] to calculate surface fluxes under the Representative
86 Concentration Pathway (RCP) 8.5 (i.e. a business-as-usual climate change scenario). Wind speed
87 and air temperature data are 6-hourly, whereas radiative and evaporation/precipitation fluxes are
88 daily. We consider two future scenarios differing in the driving oceanic conditions. For these we
89 use two global NEMO configurations, both forced by HADGEM2 data: ORCA1 (nominal 1°, 64
90 levels; identified as experiment E1) and ORCA025 (nominal 1/4°, 75 levels; identified as
91 experiment E2) [Aksenov *et al.*, 2017; Yool *et al.*, 2015; Yool *et al.*, 2013]. In both cases, surface
92 salinity in the global model is relaxed to that of HADGEM2. We linearly transform these forcing
93 data from the climate model 360-day year to the actual 365(6)-day year to give the correct
94 relationship between seasonal and tidal phases. Tidal and riverine forcing, and Baltic inflow
95 follow O'Dea *et al* [2012] and are not modified by the future climate scenario.

96 We initialise these AMM7 simulations from the driving global ocean model state at 1970
97 and run forward for 130 years to 2099 (nominal dates). We analyse the 120-year period 1980-
98 2099, taking 30-year means over 1980-2009 to be representative of present day and 2070-2099
99 to be representative of end of the century conditions. The E1 AMM7 simulation is run coupled to
100 a generic functional type ecosystem model (ERSEM [Blackford *et al.*, 2004; Edwards *et al.*,
101 2012]) and is used to illustrate some wider consequences of the changes in circulation. This
102 simulates the cycling of C, N, P and Si through multiple phyto-, zooplankton, bacteria and
103 detritus classes. Experiment E1 takes oceanic boundary conditions from the MEDUSA global
104 ecosystem model [Yool *et al.*, 2015] run in ORCA1.

105 Inherent in any climate projection are multiple uncertainties, which arise from the
 106 radiative forcing scenario, the global and regional models' structure and parameters and the
 107 natural variability masking the climate change signal [Hawkins and Sutton, 2009]. Forced model
 108 simulations explore the system's response given specified external conditions. However, the
 109 ocean state driving the atmosphere is different from that of the driven ocean model; raising
 110 issues of scenario consistency (Fig. S3). That said, this approach is well tried and tested in the
 111 context of global and regional forecast models, and so can provide dynamically sound, plausible
 112 future states. To some extent, this is supported by validation by observations. Comprehensive
 113 validation in numerical weather prediction model forced simulations is given by *O'Dea et al*
 114 [2012] for the hydrodynamics component and by *Edwards et al* [2012] for the ecosystem. New
 115 biases can be introduced by the climate model forcing. The hydrodynamic simulation (mean
 116 1980-2009) remains accurate compared with WOA09 climatology [Antonov et al., 2010], with
 117 the seasonal surface salinity showing spatial $R^2=0.7$, percentage bias (model minus observations)
 118 of 1.1% and the root mean squared error scaled by the standard deviation of the observations
 119 (RMSE/ σ_{obs}) of 0.7. However, biases in the seasonal nutrient fields introduced by initialisation
 120 by the driving global model are significantly increased compared with *Edwards et al* [2012],
 121 with percentage bias increasing from 21% to 42%, and RMSE/ σ_{obs} from 0.7 to 1.4. Spatial
 122 patterns are still reasonable, with $R^2=0.3$ compared with 0.4 for *Edwards et al* [2012].

123 2.2 Geostrophic dynamics

124 We calculate the full geostrophic transport, Q_g , by integrating the thermal wind equation
 125 downwards from the sea surface slope and a local geostrophic component, Q_{gl} , by integrating the
 126 thermal wind equation up-wards from zero velocity at the sea bed; a condition commonly used in
 127 shelf-sea observational analysis [Hill, 1996]. Hence, the full and local geostrophic velocities are
 128 defined as:

$$129 \quad u_g = \frac{g}{f} \left[-\zeta_y - \frac{1}{\rho_0} \int_z^\zeta \rho_y dz' \right] \quad u_{gl} = \frac{g}{f \rho_0} \int_{-h}^z \rho_y dz', \quad (1)$$

130 where u is the component of flow across a section, subscript y indicates an along-section
 131 derivative, g is gravitational acceleration, f is the Coriolis parameter, ρ is density, ρ_0 , a reference
 132 density, z the positive upwards vertical coordinate, ζ is the sea surface height and h is the
 133 undisturbed water depth. Transports are defined as integrals in depth and along the section
 134 (length, L): $Q = \int_0^L \int_{-h}^\zeta u dz dy$. The difference between Q_g and Q_{gl} gives the remote geostrophic
 135 component, Q_{gr} . Hence, with a local wind-driven Ekman term ($Q_{ek}=\tau L/f$), for wind stress τ , and
 136 a residual, Q_{res} , the full decomposition is:

$$137 \quad Q = Q_g + Q_{ek} + Q_{res} = Q_{gl} + Q_{gr} + Q_{ek} + Q_{res}. \quad (2)$$

138 The residual, Q_{res} , accounts for advection, bottom friction and calculation uncertainty. If
 139 we identify the component of the sea surface slope, ζ_{ly} , consistent with u_{gl} at the surface, then for
 140 zero net pressure gradient at the sea bed (with $u_{gr}=u_g-u_{gl}$):

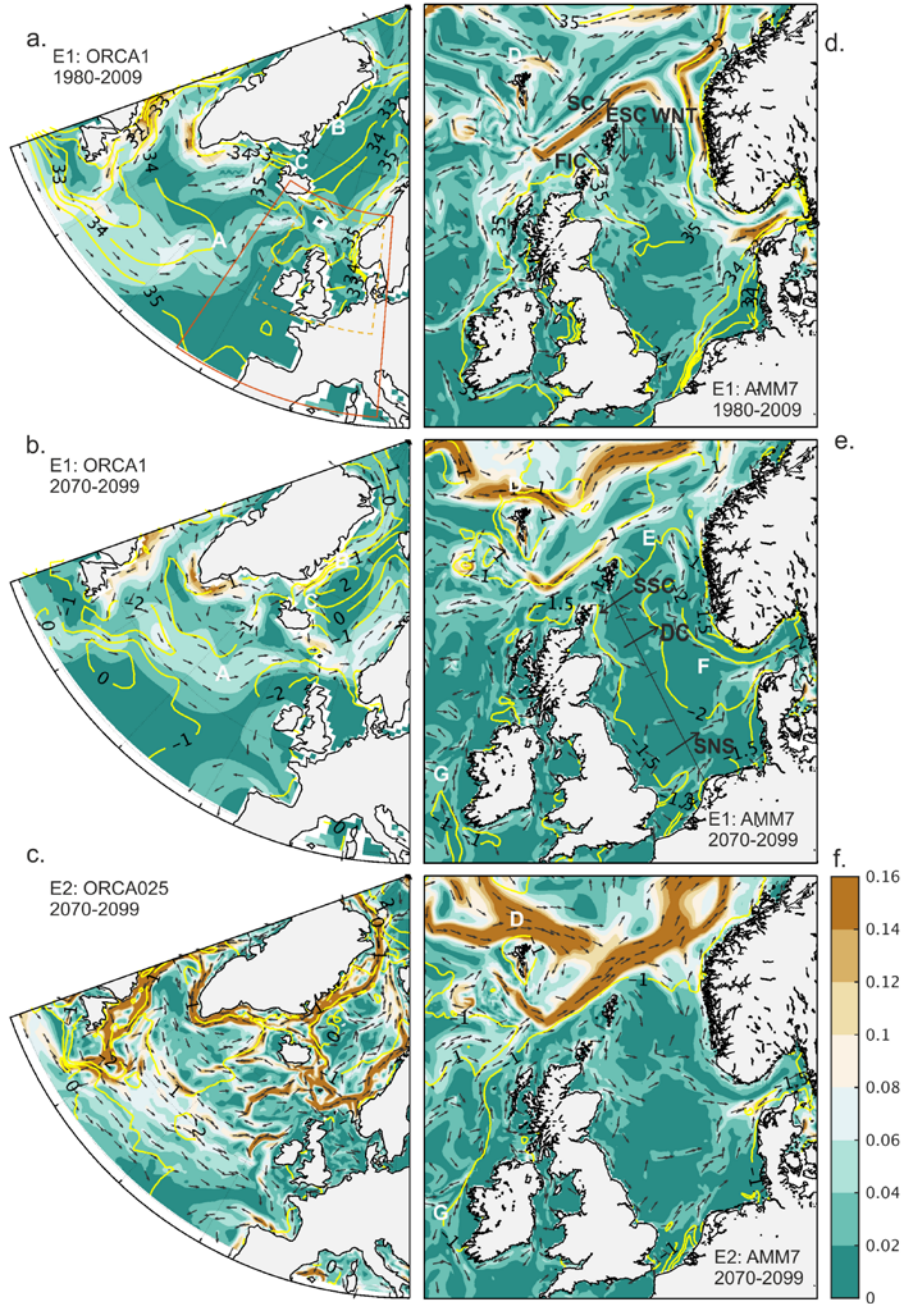
$$141 \quad \zeta_{ly} = -\frac{1}{\rho_0} \int_{-h}^\zeta \rho_y dz', \quad \zeta_y = \zeta_{ly} + \zeta_{ry}, \quad \text{and} \quad u_{gr} = -\frac{g}{f} \zeta_{ry}. \quad (3)$$

142 Hence, the local and remote geostrophic transports can be interpreted as arising
 143 respectively from local density gradients and from non-local currents propagating as a barotropic
 144 sea-surface slope signal. The observed value of Q_{gl} can be calculated from CTD profiles along
 145 the sections. The section estimating the inflow on the western flank of the Norwegian Trench

146 (WNT; Fig. 1) has been occupied 37 times between 1977 and 2016. We select profiles for each
147 transect from the EN4.2 database [*Good et al.*, 2013] within 0.1° of the section and taken within
148 14 days. These are interpolated onto a 2m vertical grid and geostrophic currents estimated by a
149 finite difference approach. This gives a mean observed Q_{gl} of -0.12Sv (northward), ranging from
150 -0.47 to 0.28Sv .
151

152

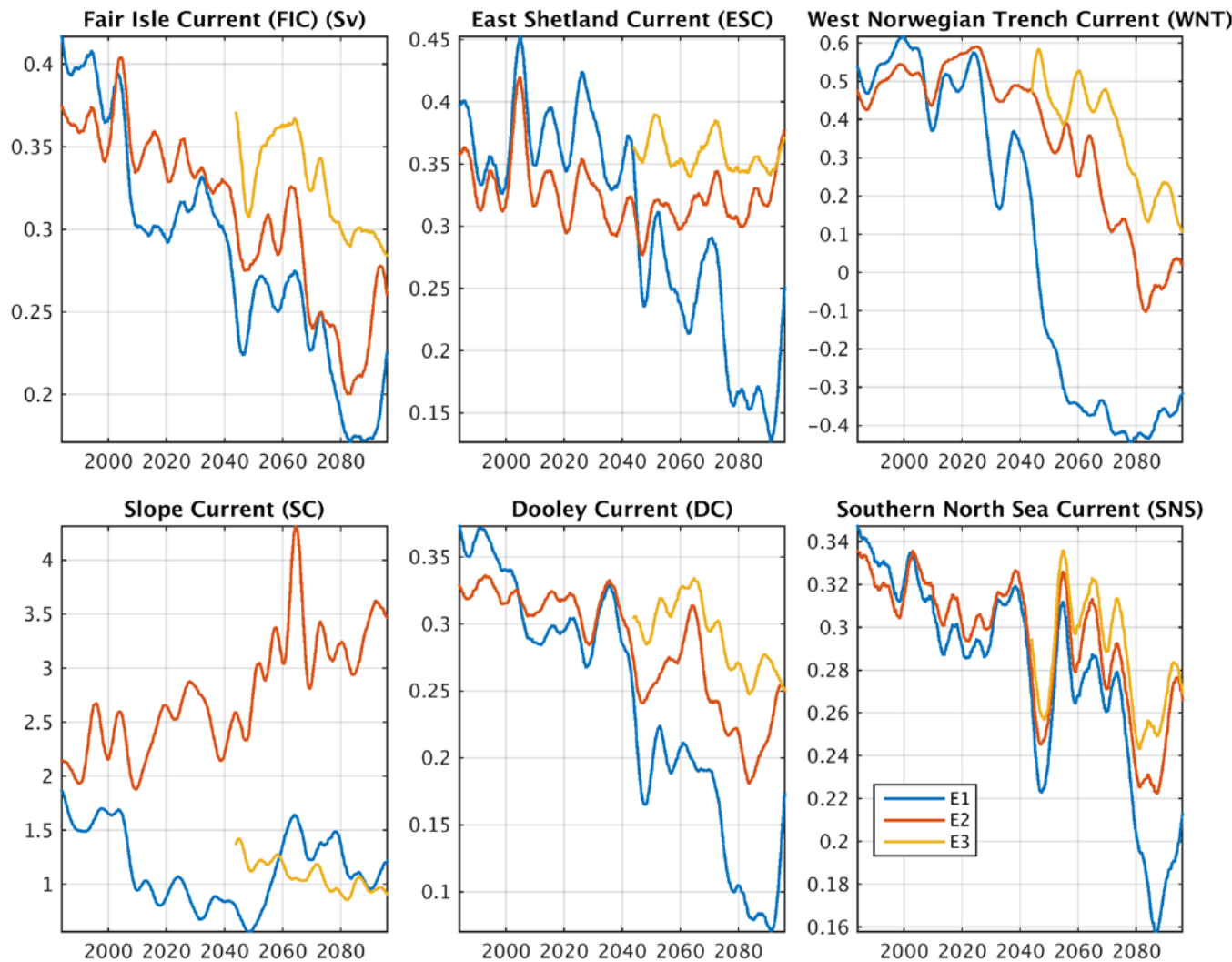
153



154

155 **Figure 1.** Depth mean currents (0 to 200m) from the two driving global NEMO models (a-c) and
 156 downscaled results (d-f) for a sub-region (dashed box on a.) of the regional model (solid on a.,
 157 and Fig. S1). Colours show speed (ms^{-1}) and arrows show direction. Top figures show mean
 158 present-day conditions, centre (E1) and bottom (E2) show mean end-of-century conditions.
 159 Yellow contours in (a,d) show surface salinity, and in (b,c,e,f) show the salinity differences
 160 between future and present. (d-e) also show the sections used for time-series and geostrophic
 161 analysis (Figs. 2, 3), with arrows indicating the direction of positive transport.

162



163

164 **Figure 2** Time-series of volume transport (Sv) for six sections on Fig. 1. Monthly data is
 165 Gaussian filtered, $\sigma=2$ years. Experiment E3 is restarted from E1 at 2040 with ocean boundary
 166 conditions taken from 1980-2009.

167 3. Changes to the North Sea circulation under future climate scenarios

168 In the two future scenarios considered here (E1 and E2), the transport along all three
 169 pathways of Atlantic flow into the North Sea [Sheehan *et al.*, 2017; Turrell *et al.*, 1996] is
 170 substantially reduced compared with present day conditions (Figs. 1, 2). The Fair Isle Current
 171 (FIC) decreases by 48% in E1 and 35% in E2; and the East Shetland Current (ESC) decreases by
 172 50% in E1, remaining largely unchanged in E2. The flow on the western flank of the Norwegian
 173 Trench (WNT) decreases by 173%, reversing sign in E1 during a key event over 2040-2057. In
 174 E2, WNT decreases sharply from 2040 to near zero by 2080 (by 94%). The strong poleward
 175 flowing boundary current of the North Atlantic sub-polar gyre (the Slope Current) feeds the
 176 WNT inflow. In both experiments, the slope current largely bypasses the North Sea in the end-
 177 of-century period and instead continues straight towards the Norwegian Sea. The decrease in

178 inflow reduces the cyclonic circulation of the North Sea, notably the Dooley Current (Figs. 1, 2)
179 by 68% in E1 and 31% in E2.

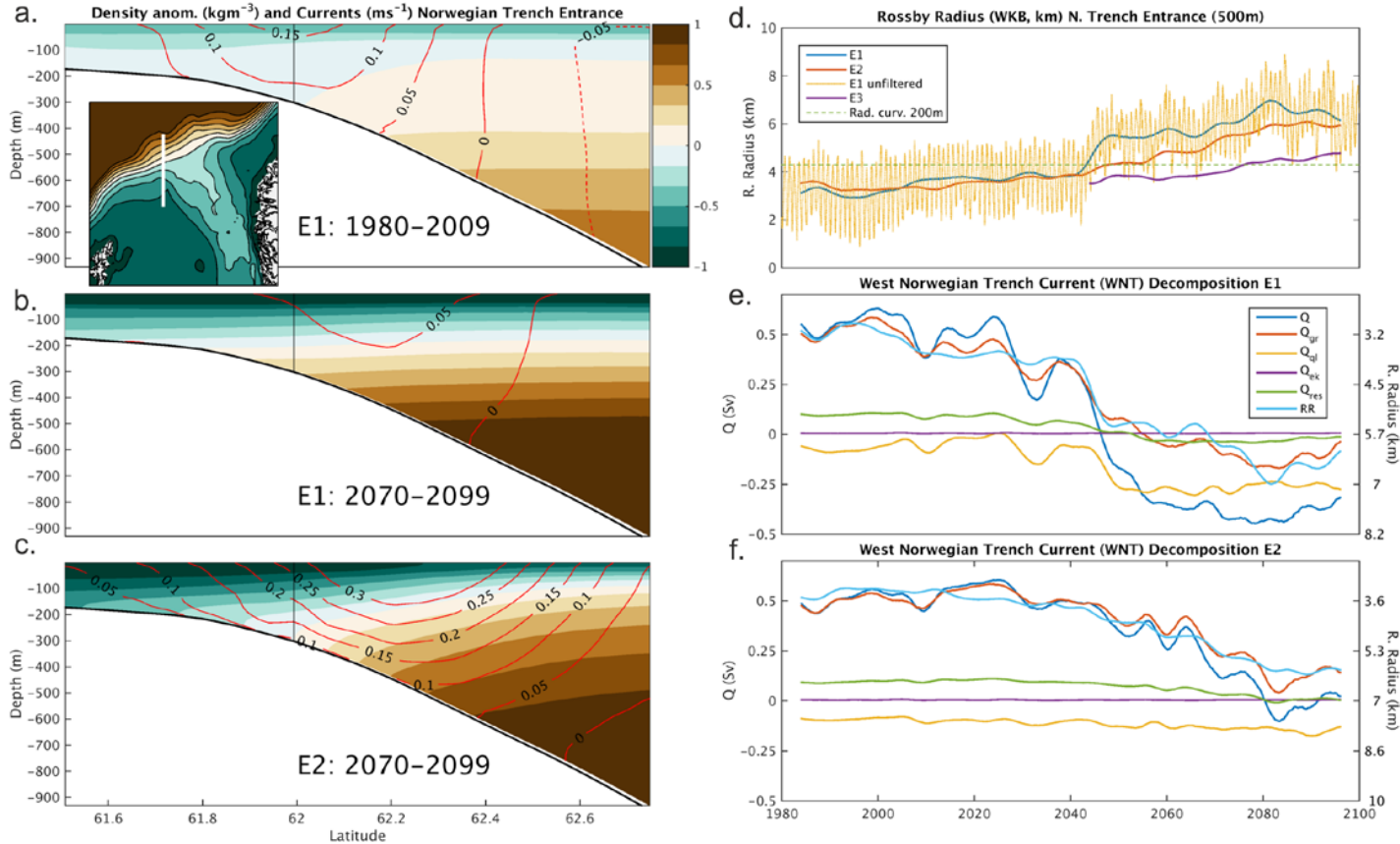
180 The changes in North Sea circulation are accompanied by a substantial freshening of this
181 sea and an increase in the salinity (and density) contrast between the shelf-sea and the open
182 ocean (Fig. 1e-f); a reduced inflow of saltier Atlantic water leads to the North Sea containing an
183 increased fraction of riverine freshwater. We confirm the dominant role of wider oceanographic
184 conditions in driving the circulation and density changes through an experiment that matches E1
185 but with present-day oceanic boundary conditions (E3; Figs. 2, 3c). This shows North Sea
186 inflows that are reduced by a much smaller fraction than in E1: FIC by 22% rather than 48%;
187 WNT by 54% rather than 173% and ESC by 7% rather than 50%. HADGEM2 shows a 15%
188 decrease in wind-stress over these shelf-seas by the end of the century, which accounts for the
189 modest decrease in inflow in E3.

190 These dramatic changes in the North Sea coincide with some substantial changes in the
191 gyre circulation and salinity in the North Atlantic and Nordic Seas (Fig. 1a-c). In E1 and E2
192 future scenarios, the northeastward North Atlantic Current (labelled A) is fresher and positioned
193 farther north than in present conditions. In the Nordic Seas, the East Greenland Current
194 intensifies (B on Fig. 1a). On reaching Iceland, this current bifurcates (at C): one branch
195 accelerates the East Iceland Current and one mixes with the Irminger Current and joins the North
196 Atlantic current near Newfoundland. Currents are substantially stronger in E1 than in E2 [*Yool et*
197 *al.*, 2015] and this is evident in the boundary conditions driving the regional model (Fig. S2).
198 Under present day conditions, the East Iceland Current (Fig. 1d labelled D) crosses the southern
199 Norwegian Sea and leaves the region without contact with the northwest European shelf
200 [*Jakobsen et al.*, 2003], apart from a weak flow east of Faroe. Under the future scenarios (E1 and
201 E2; Fig. 1e-f) the enhanced East Iceland Current flows southwest, joining the slope current,
202 carrying water 0.5-1.0 units fresher than in present-day conditions. In E2, this is substantially
203 intensified and also joins the slope current further north, enhancing the along-slope density
204 gradient.

205 **3.1 Diagnosing the circulation changes**

206 The decrease in the western Norwegian Trench inflow (WNT) in E1 and E2, and in the
207 East Shetland Current (ESC) inflow in E1, can be traced to the substantial increase in surface
208 stratification at the entrance to the Norwegian Trench (Fig. 3a-c). The mean buoyancy frequency
209 here increases by a factor of 2.0 in E1 and 1.4 in E2 and the minimum Rossby radius increases
210 (Fig. 3d) to consistently exceed the mean radius of curvature of the entrance (~4.3 km). The
211 Rossby radius characterises the length scale of deviations of flow from topographic steering
212 under the Taylor-Proudman theorem [*Hide*, 1971]. Hence, as the Rossby radius increases with
213 increasing stratification and exceeds the length scale of the topography, this steering is relaxed
214 and a decreasing fraction of the slope current turns the sharp corner into the Norwegian Trench
215 (Fig. 1e labelled E). The core of the slope current moves oceanwards and the slope current
216 largely bypasses the Norwegian Trench (Figs. 1d-f and 3a-c). In scenario E2, the strong increase
217 in density gradient along the slope in the Faeroe-Shetland channel accelerates the slope current
218 [*Huthnance*, 1984] (Fig. S6 and Eqn. S3). This acceleration mitigates the decrease in WNT in
219 E2. In experiment E1, in contrast, the slope current weakly decreases.

220



221
 222 **Figure 3.** Latitude-Depth cross-sections of density anomaly (colours) and velocity
 223 (contours) at the entrance to the Norwegian Trench in E1: Present (a) and Future (b), and E2:
 224 Future (c). The vertical line indicates the depth of the deepest isobath that turns the corner to
 225 enter the Norwegian Trench. The insert shows isobaths at this entrance and the location of this
 226 section. The inflow is diagnosed using time-series (d) of Rossby radius (1st baroclinic, estimated
 227 from WKB approximation [*Chelton et al.*, 1998]) at the 500m isobath for E1, E2 and E3 and the
 228 geostrophic decomposition (Eqn 2) for E1 (e) and E2 (f), filtered as in Fig. 2.

229
 230 The geostrophic decomposition for WNT (Fig. 3e-f; see Figs. S4, S5 for other sections)
 231 shows that the non-local geostrophic component (Q_{gr}), relating to the barotropic sea-surface
 232 slope, decreases markedly (from $Q_{gr}=0.51\text{Sv}$ to -0.12Sv in E1 and from 0.50 to 0.16Sv in E2).
 233 This component scales very closely with the Rossby Radius at the entrance ($R^2=0.97$ and 0.91 in
 234 E1 and E2), strongly supporting the above explanation that relaxation of topographic steering
 235 leads to the reduction in WNT.

236 Repeat-section CTD observations across WNT show the local geostrophic current is
 237 northwards here, with $Q_{gl} = -0.12\text{Sv}$, somewhat larger than the modelled value of -0.07Sv in E1.
 238 In the future period, this increases to -0.26Sv (Fig. 3f) as the weaker WNT allows more
 239 freshwater from near the coast of continental Europe to flow northwards (Fig. 1 labelled F, and
 240 Figs. S6,S7), seen as a 2.0 unit salinity deficit. This further increases the density gradient across
 241 the western slope of the Norwegian Trench, enhancing the northward Q_{gl} . This positive feedback
 242 leads to a substantial increase in the now northward WNT, and the North Sea circulation has

243 entered a new state. This new circulation state (see also [Tinker *et al.*, 2016]) can be seen as
 244 naturally arising from the usual density field, but in present conditions is inhibited by external
 245 barotropic currents (see Figs. S6,S7). In E2, Q_{gr} for WNT also closely scales with the Rossby
 246 radius at the entrance to the Norwegian Trench and Q_{gl} also increases, from -0.09 to -0.15Sv
 247 (Fig. 3f). However, the total transport (Q) remains southward, due to the acceleration of the slope
 248 current, and the runaway feedback with northwards freshwater transport is not initiated.

249 The decrease in the East Shetland Current (ESC) seen in E1, but not in E2, arises because
 250 the northwards freshwater transport reaches the northern North Sea (cold/salty) density
 251 maximum, which is removed in this scenario (Fig. S6). Without this density maximum the local
 252 geostrophic component of the South Shetland Current and Dooley Current is reduced (Q_{gl}
 253 decreases from 0.12 to 0.01Sv and from 0.15 to 0.08Sv respectively), and consequently the ESC
 254 substantially decreases. The reduction in ESC further reduces the salinity and another positive
 255 feedback is established. In E2 the freshwater does not reach the density maximum (Fig. S6) and
 256 the ESC remains largely unchanged. Hence, the key difference between E1 and E2 lies in
 257 whether the changes in Western Norwegian Trench inflow are sufficient to disrupt the northern
 258 North Sea density distribution and so impact the ESC.

259 The consistent decrease in the Fair Isle Current (FIC; Fig. 2) in both E1 and E2 can be
 260 traced upstream to the reversal in the shelf current west of Ireland (Fig. 1e-f labelled G) and in
 261 turn to ocean-shelf transport in the Celtic Sea. Drifter observations show a continuous flow
 262 pathway from the Celtic Sea to the Fair Isle channel [Pingree *et al.*, 1999]. The northward shift
 263 of the North Atlantic Current and its decreasing salinity (Fig. 1a-c) leads to a negative poleward
 264 density gradient, reducing the slope current. The resulting off-shelf geostrophic component (Fig
 265 S8 and Eqn. S2) inhibits the usual eastward wind driven on-shelf flow.

266 Hence, we identify two key external drivers to these changes in North Sea circulation in
 267 E1 and E2: a substantial increase in stratification in the Faeroe-Shetland Channel (for WNT and
 268 for ESC in E1) and a reduction in poleward density gradient due to freshening of the North
 269 Atlantic current (for FIC). The increase in stratification is primarily due to reduced surface
 270 salinity (65% in E1 and 75% in E2; based on Eqn S1). This cannot be accounted for by changes
 271 in surface freshwater flux (which increases by only 10%), and hence arises from lateral transport.
 272 The Faeroe-Shetland channel receives surface water from both the North Atlantic Current
 273 (eastward) and the East Icelandic Current (southward). The surface salinity of both decreases
 274 steadily. However, a lagged, detrended correlation shows the variability of WNT in E1 relates
 275 much more strongly with the surface salinity of the East Icelandic Current (max $R^2=0.70$, at lag
 276 14 months) compared with that of the North Atlantic Current (maximum $R^2=0.05$, at lag 26
 277 months). For E2 this is less clear: maximum $R^2=0.24$ at 24 months (southward) and 0.50 at 33
 278 months (eastward). We would expect the wider oceanic changes identified here to be related to
 279 changes in Arctic sea ice and circulation, sub-polar gyre salinity and circulation, and the Atlantic
 280 meridional overturning circulation. We leave further investigation of the underlying mechanisms
 281 in the coupled ocean-atmosphere-cryosphere system to future work. However, It is worth noting
 282 that the substantial change in WNT coincides with the accelerating loss of Arctic sea ice and an
 283 ice-free East Greenland Current in the driving models [Aksenov *et al.*, 2017].

284 **3.2 How likely is this shutdown scenario?**

285 The CMIP5 ensemble [Taylor *et al.*, 2012] enables an estimate of the likelihood of these
 286 circulation changes occurring, through linear relations between North Sea inflows and boundary

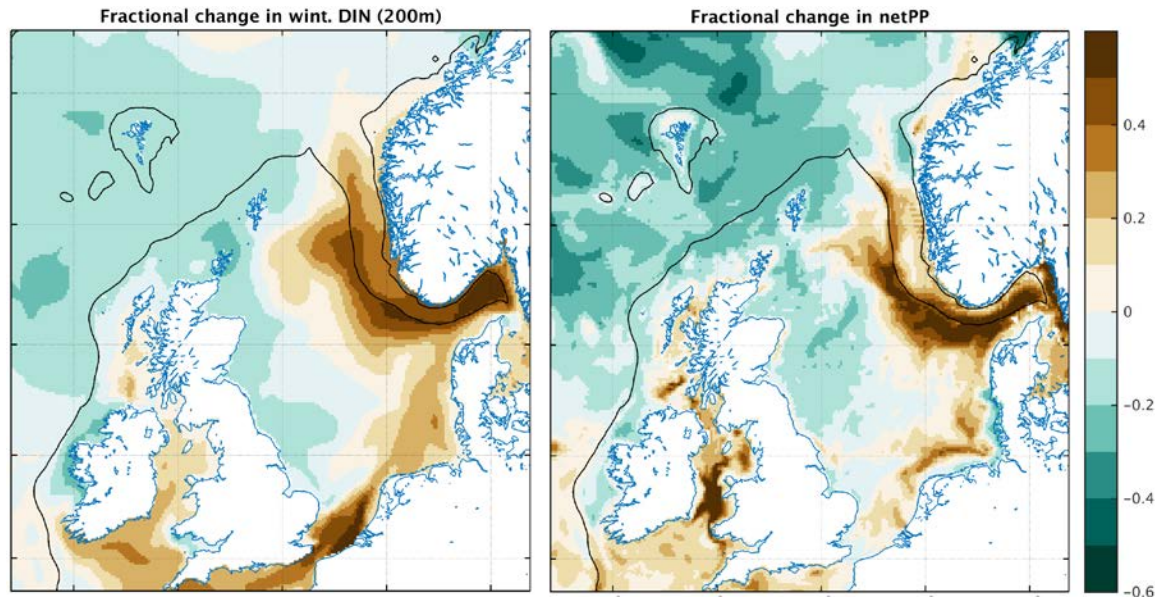
287 condition properties, identified above as key drivers of these changes (available for WNT and
288 FIC; Supplement 3). Applying these linear relationships to 22 CMIP5 simulations, 20 and 18
289 ensemble members show a decrease in FIC and WNT inflows respectively. Compared with this
290 distribution, the decreases in E2 are -0.37σ and -1.0σ from the median CMIP5 change for FIC
291 (-0.09Sv) and WNT (-0.18Sv). There is less similarity between CMIP5 and E1, which gives
292 decreases of -1.0σ and -2.7σ . Applying these relations to HADGEM2, used for atmospheric
293 forcing, shows a similar decreases to E2 for WNT ($-0.57\text{Sv} = -1.4\sigma$), but no significant change
294 for FIC. This arises because HADGEM2 and NEMO have different dynamics and mixing
295 characteristics, leading to different deep-water mass properties (Fig. S3). Given the inherent
296 uncertainty of the density and circulation in climate models at high latitudes, this analysis is itself
297 uncertain, but provides useful guidance that these processes need to be considered among the
298 significant marine climate impacts in this region.

299 We evaluate whether a reduction in oceanic inflow might be a potential impact of climate
300 change in other regions globally using the high-resolution global model (E2), which itself shows
301 a $\sim 60\%$ reduction in North Sea inflow. However, we find no evidence of a comparable reduction
302 in inflow, in other shelf-seas around the world. This suggests that the combination of oceanic
303 change and the particular North Sea geometry makes such an inflow reduction unique to this
304 region. That said, increasing ocean stratification is a robust outcome of future climate projections
305 [Capotondi *et al.*, 2012], suggesting that decoupling of currents from topographic steering
306 arising from geostrophic theory [Hide, 1971] could become more widespread, though perhaps at
307 a smaller scale than seen here in the North Sea.

308 **3.3 Implications for the North Sea**

309 With reduced inflow, a shelf-sea becomes less influenced by oceanic and more by
310 riverine inputs, which are constant in these experiments. Considering dissolved inorganic
311 nitrogen (DIN), we turn to results from the biogeochemical model run with E1, Fig. 4. The
312 western side of the North Sea shows a decrease in winter DIN reflecting reduced oceanic values
313 being advected on-shelf; a consequence of the established open-ocean reduction in nutrients due
314 to increased stratification [Bopp *et al.*, 2013; Gröger *et al.*, 2013; Holt *et al.*, 2012]. In contrast,
315 the southern and eastern regions show a marked increase as they ‘fill-up’ with riverine water of
316 higher DIN concentration. Based on a well-mixed, steady-state estimate [Holt *et al.*, 2012] the
317 riverine contribution to DIN across the whole North Sea increases from $\sim 8\%$ to $\sim 30\%$. These
318 changes in winter DIN are matched by a corresponding change in annual net primary production
319 (Fig. 4), suggesting an enhanced risk of coastal eutrophication and summer near-bed oxygen
320 depletion events in stratified regions [Ciavatta *et al.*, 2016; Queste *et al.*, 2013]. However,
321 increases in the southern North Sea are partly mitigated by light limitation and decreases in the
322 north and west are augmented by local increases in summer stratification [Holt *et al.*, 2016].
323 Wider ecosystem impacts might also be expected. Certain commercially and ecologically
324 important species have life cycles coupled to the North Sea circulation; e.g. Herring larvae rely
325 on the cyclonic circulation for transport from spawning to nursery grounds [Corten, 2013] and
326 deep-water coral *Lophelia pertusa* larvae are advected between oil/gas platforms, which they
327 colonise [Henry *et al.*, 2018]. Moreover, the consequent increase in flushing time in these
328 scenarios implies anthropogenic pollutants would be retained for longer, enhancing local impact
329 and the risk of bioaccumulation.

330



331

332 **Figure 4** Fractional change (Future/Present-1) of winter Dissolved Inorganic Nitrogen
 333 (DIN) and annual net Primary Production (netPP) from the ERSEM ecosystem model in E1.

334 4. Conclusion

335 Here we demonstrate how large-scale changes in ocean circulation and hydrography can
 336 have marked impacts on shelf-sea currents through a combination of stratification, geostrophic
 337 and feedback processes that are not currently captured by global climate models, nor have they
 338 been the focus of local climate impact studies. Circulation changes, such as the shutdown event
 339 identified here, would have wide-ranging impacts on shelf-sea ecosystems and the resources and
 340 services that rely on these. It is crucial, therefore, that climate change impacts of larger-scale
 341 oceanographic drivers are considered alongside the more widely investigated impacts of
 342 warming, sea level rise and ocean acidification.

343 Acknowledgments

344 This work was supported by NOC and PML's National Capability programme in Ocean
 345 Modelling. It was also supported by the UK Natural Environmental Research Council research
 346 grants: FASTNet (NE/I030259/1), ROAM (NE/H01733X/1) and RECICLE (NE/M003477/1),
 347 and by the EU FP7 projects MYOCEAN and EuroBASIN. High Performance computing was
 348 provided by the UK Research Councils' facility ARCHER. Data from these simulations will be
 349 made available via the NERC JASMIN data server.

350 References

- 351 Adlandsvik, B. (2008), Marine downscaling of a future climate scenario for the North Sea, *Tellus Ser. A-Dyn.*
 352 *Meteorol. Oceanol.*, 60(3), 451-458.
- 353 Aksenov, Y., E. E. Popova, A. Yool, A. J. G. Nurser, T. D. Williams, L. Bertino, and J. Bergh (2017), On the future
 354 navigability of Arctic sea routes: High-resolution projections of the Arctic Ocean and sea ice, *Marine Policy*,
 355 75(Supplement C), 300-317.

- 356 Antonov, J. I., D. Seidov, T. P. Boyer, R. A. Locarnini, A. V. Mishonov, H. E. Garcia, O. K. Baranova, M. M.
 357 Zweng, and J. D.R. (2010), World Ocean Atlas 2009, Volume 2: Salinity *Rep.*, 184pp pp, U.S. Government Printing
 358 Office, Washington, D.C.
- 359 Blackford, J. C., J. I. Allen, and F. J. Gilbert (2004), Ecosystem dynamics at six contrasting sites: a generic model
 360 study, *Journal of Marine Systems*, 52, 191-215.
- 361 Bopp, L., et al. (2013), Multiple stressors of ocean ecosystems in the 21st century: projections with CMIP5 models,
 362 *Biogeosciences*, 10(10), 6225-6245.
- 363 Capotondi, A., M. A. Alexander, N. A. Bond, E. N. Curchitser, and J. D. Scott (2012), Enhanced upper ocean
 364 stratification with climate change in the CMIP3 models, *J. Geophys. Res.-Oceans*, 117, C04031.
- 365 Chelton, D. B., R. A. deSzoeke, M. G. Schlax, K. El Naggar, and N. Siwertz (1998), Geographical Variability of the
 366 First Baroclinic Rossby Radius of Deformation, *Journal of Physical Oceanography*, 28(3), 433-460.
- 367 Ciavatta, S., S. Kay, S. Saux-Picart, M. Butenschön, and J. I. Allen (2016), Decadal reanalysis of biogeochemical
 368 indicators and fluxes in the North West European shelf-sea ecosystem, *Journal of Geophysical Research: Oceans*,
 369 121, 1824-1845.
- 370 Corten, A. (2013), Recruitment depressions in North Sea herring, *ICES Journal of Marine Science*, 70(1), 1-15.
- 371 Edwards, K. P., R. Barciela, and M. Butenschon (2012), Validation of the NEMO-ERSEM operational ecosystem
 372 model for the North West European Continental Shelf, *Ocean Sci.*, 8(6), 983-1000.
- 373 Good, S. A., M. J. Martin, and N. A. Rayner (2013), EN4: Quality controlled ocean temperature and salinity profiles
 374 and monthly objective analyses with uncertainty estimates, *Journal of Geophysical Research: Oceans*, 118(12),
 375 6704-6716.
- 376 Gröger, M., E. Maier-Reimer, U. Mikolajewicz, A. Moll, and D. Sein (2013), NW European shelf under climate
 377 warming: implications for open ocean and shelf exchange, primary production, and carbon absorption,
 378 *Biogeosciences*, 10(6), 3767-3792.
- 379 Hawkins, E., and R. Sutton (2009), The potential to narrow uncertainties in regional climate predictions, *Bulliten of*
 380 *the American Meteorological Society*, 90, 1095-1107.
- 381 Henry, L.-A., C. G. Mayorga-Adame, A. D. Fox, J. A. Polton, J. S. Ferris, F. McLellan, C. McCabe, T. Kutti, and J.
 382 M. Roberts (2018), Ocean sprawl facilitates dispersal and connectivity of protected species, *Scientific Reports*, 8(1),
 383 11346.
- 384 Hide, R. (1971), On geostrophic motion of a non-homogeneous fluid, *Journal of Fluid Mechanics*, 49(4), 745-751.
- 385 Hill, A. E. (1996), Spin Down and the dynamics of Dense Pool Gyres in Shallow Seas, *Journal of Marine Research*,
 386 54, 471-486.
- 387 Holt, J., M. Butenschon, S. L. Wakelin, Y. Artioli, and J. I. Allen (2012), Oceanic controls on the primary
 388 production of the northwest European continental shelf: model experiments under recent past conditions and a
 389 potential future scenario, *Biogeosciences*, 9(1), 97-117.
- 390 Holt, J., et al. (2016), Potential impacts of climate change on the primary production of regional seas: a comparative
 391 analysis of five European seas *Progress in Oceanography*, 140, 91-115.
- 392 Holt, J., et al. (2017), Prospects for improving the representation of coastal and shelf seas in global ocean models,
 393 *Geosci. Model Dev.*, 10(1), 499-523.
- 394 Huthnance, J. M. (1984), Slope Currents and Jebar, *Journal of Physical Oceanography*, 14(4), 795-810.
- 395 Jakobsen, P. K., M. H. Ribergaard, D. Quadfasel, T. Schmith, and C. W. Hughes (2003), Near-surface circulation in
 396 the northern North Atlantic as inferred from Lagrangian drifters: Variability from the mesoscale to interannual, *J.*
 397 *Geophys. Res.-Oceans*, 108(C8).
- 398 Jones, C. D., et al. (2011), The HadGEM2-ES implementation of CMIP5 centennial simulations, *Geosci. Model*
 399 *Dev.*, 4(3), 543-570.

- 400 Large, W. G., and S. Yeager (2004), Diurnal to decadal global forcing for ocean and sea-ice models: the data sets
401 and flux climatologies. NCAR Technical Note NCAR/TN-460+STR, doi:10.5065/D6KK98Q6.Rep.
- 402 Madec, G. (2008), *NEMO reference manual, ocean dynamic component: NEMO-OPA. Note du Pole de*
403 *modelisation, Institut Pierre Simon Laplace, Technical Report 27, ISSN No, 1288-1619.*
- 404 O'Dea, E. J., et al. (2012), An operational ocean forecast system incorporating NEMO and SST data assimilation for
405 the tidally driven European North-West shelf, *Journal of Operational Oceanography*, 5(1), 3-17.
- 406 Pingree, R. D., B. Sinha, and C. R. Griffiths (1999), Seasonality of the european slope current (Goban Spur) and
407 ocean margin exchange, *Continental Shelf Research*, 19, 929-975.
- 408 Quante, M., and F. Colijn (2016), *North Sea Region Climate Change Assessment*, 429 pp., Springer.
- 409 Queste, B. Y., L. Fernand, T. D. KJickells, and K. J. Heywood (2013), Spatial extent and historical context of North
410 Sea oxygen depletion in August 2010, *Biogeochemistry*, 113, 53-68.
- 411 Schrum, C., J. Lowe, H. E. M. Meier, I. Grabemann, J. Holt, M. Mathis, T. Pohlmann, M. D. Skogen, A. Sterl, and
412 S. Wakelin (2016), Projected Change—North Sea, in *North Sea Region Climate Change Assessment*, edited by M.
413 Quante and F. Colijn, pp. 175-217, Springer International Publishing, Cham.
- 414 Sheehan, P. M. F., B. Berx, A. Gallego, R. A. Hall, K. J. Heywood, and S. L. Hughes (2017), Thermohaline forcing
415 and interannual variability of northwestern inflows into the northern North Sea, *Continental Shelf Research*, 138,
416 120-131.
- 417 Taylor, K. E., R. J. Stouffer, and G. A. Meehl (2012), An Overview of CMIP5 and the Experiment Design, *Bulletin*
418 *of the American meteorological society (BAMS)* 93, 485–498. .
- 419 Thomas, H., Y. Bozec, K. Elkalay, and H. J. W. de Baar (2004), Enhanced Open Ocean Storage of CO₂ from Shelf
420 Sea Pumping, *Science* 304, 1005-1008.
- 421 Tinker, J., J. Lowe, A. Pardaens, J. Holt, and R. Barciela (2016), Uncertainty in climate projections for the 21st
422 century northwest European shelf seas, *Progress in Oceanography*, 148, 56-73.
- 423 Turrell, W. R., G. Slessor, R. Payne, R. D. Adams, and P. A. Gillibrand (1996), Hydrography of the East Shetland
424 Basin in relation to decadal North Sea variability, *ICES Journal of Marine Science*, 53(6), 899-916.
- 425 Yool, A., E. E. Popova, and A. C. Coward (2015), Future change in ocean productivity: Is the Arctic the new
426 Atlantic?, *Journal of Geophysical Research: Oceans*, 120(12), 7771-7790.
- 427 Yool, A., E. E. Popova, A. C. Coward, D. Bernie, and T. R. Anderson (2013), Climate change and ocean
428 acidification impacts on lower trophic levels and the export of organic carbon to the deep ocean, *Biogeosciences*,
429 10(9), 5831-5854.
- 430
- 431